LETTERS
https://doi.org/10.1038/s41567-020-0816-x

nature physics

Proximity-induced superconducting gap in the quantum spin Hall edge state of monolayer WTe_2

Felix Lüpke[1,5,6], Dacen Waters[1,6], Sergio C. de la Barrera[1], Michael Widom[1], David G. Mandrus[2,3,4], Jiaqiang Yan[2], Randall M. Feenstra[1] and Benjamin M. Hunt[1] ✉

The quantum spin Hall insulator is characterized by a bandgap in the two-dimensional (2D) interior and helical 1D edge states[1–3]. Inducing superconductivity in the helical edge state results in a 1D topological superconductor, a highly sought-after state of matter at the core of many proposals for topological quantum computing[4]. In the present study, we report the coexistence of superconductivity and the quantum spin Hall edge state in a van der Waals heterostructure, by placing a monolayer of 1T′-WTe_2, a quantum spin Hall insulator[1–3], on a van der Waals superconductor, $NbSe_2$. Using scanning tunnelling microscopy and spectroscopy (STM/STS), we demonstrate that the WTe_2 monolayer exhibits a proximity-induced superconducting gap due to the underlying superconductor and that the spectroscopic features of the quantum spin Hall edge state remain intact. Taken together, these observations provide conclusive evidence for proximity-induced superconductivity in the quantum spin Hall edge state in WTe_2, a crucial step towards realizing 1D topological superconductivity and Majorana bound states in this van der Waals material platform.

Contemporary interest in topological superconductors has been driven by potential applications of their gapless boundary excitations, which are thought to be emergent Majorana quasiparticles with non-abelian statistics[5–8]. One path toward topological superconductivity is to realize an intrinsic spinless *p*-wave superconductor[9]. A powerful alternative is to use a conventional *s*-wave superconductor to induce Cooper pairing in topologically non-trivial states via the superconducting proximity effect, resulting in an effective *p*-wave pairing[10]. This approach has recently been employed to engineer two-dimensional (2D) topological superconductivity in epitaxial 3D topological insulator films grown on a superconducting substrate[11,12] and 1D topological superconductivity by proximitizing a 2D quantum spin Hall system in buried epitaxial semiconductor quantum wells[13,14]. Although such demonstrations mark important milestones, there are clear advantages for exploring topological superconductivity in the van der Waals material platform. Using layered 2D materials allows the 2D quantum spin Hall edge to be proximitized in vertical heterostructures, circumventing the length restrictions of lateral proximity-effect geometries. Furthermore, the surfaces and edges are readily available for surface probes, allowing the detection and fundamental study of signatures of the 1D topological superconducting state. An intrinsic quantum spin Hall state has been demonstrated experimentally in monolayers of 1T′-WTe_2 (refs. [1–3,15–17]), following earlier theoretical predictions[18]. WTe_2 is attractive for studying the quantum spin Hall edge modes because it can be readily incorporated in van der Waals heterostructures and has shown quantized edge conductance up to 100 K (ref. [3]). Furthermore, monolayer WTe_2 was recently also shown to host intrinsic superconducting behaviour below ~1 K when electrostatically gated into the conduction band[19,20].

In the present work, we study mechanically exfoliated single- and few-layer WTe_2, which are transferred onto the van der Waals *s*-wave superconductor $NbSe_2$. We show that this approach induces a superconducting gap in the WTe_2 without the need for electrostatic doping and yields a critical temperature much higher than that of the intrinsic WTe_2 superconductivity, an experimental advantage that facilitates studies of the interplay of superconductivity and the quantum spin Hall edge modes. We employ scanning tunnelling microscopy (STM) and spectroscopy (STS) to investigate the proximity-induced superconducting gap as a function of temperature, magnetic field and WTe_2 thickness. By spatially resolving the spectroscopic features of the WTe_2, we find that the superconducting gap coexists with the quantum spin Hall signature at the monolayer WTe_2 edge.

We have developed a novel fabrication technique that enables the assembly and deterministic placement of van der Waals heterostructures in a glovebox (Fig. 1a). Although similar methods have been used to fabricate complex encapsulated mesoscale devices[21], critically, our technique produces atomically clean surfaces of air-sensitive materials suitable for high-resolution scanning probe measurements (for details see Supplementary Section 1). Figure 1b presents an STM image of the resulting heterostructure, where the WTe_2 monolayer edge and the underlying $NbSe_2$ are visible, showing atomically clean surfaces on each material. The profile across the step edge shows a step height of ~7 Å, which corresponds to one WTe_2 layer[17], indicating an atomically clean interface between the WTe_2 and $NbSe_2$. In Fig. 1b a weak moiré pattern can be seen; this is analysed in more detail in Supplementary Section 2. Atomically resolved STM images of the $NbSe_2$ surface (Fig. 1c) show the well-known 3×3 charge density wave[11], indicating the pristine quality of the $NbSe_2$ flake. Atomically resolved STM images of the WTe_2 (Fig. 1d) are characterized by vertical atomic rows parallel to the *a* axis of the WTe_2 unit cell.

Turning now to spectroscopic analysis of these surfaces, Fig. 2a shows a series of dI/dV spectra taken along a line perpendicular to the WTe_2 monolayer step edge (upper panel) and the corresponding height profile (lower panel). The dI/dV spectra clearly show the presence of an increased local density of states (LDOS) near the

[1]Department of Physics, Carnegie Mellon University, Pittsburgh, PA, USA. [2]Materials Science and Technology Division, Oak Ridge National Laboratory, Oak Ridge, TN, USA. [3]Department of Materials Science and Engineering, University of Tennessee, Knoxville, TN, USA. [4]Department of Physics and Astronomy, University of Tennessee, Knoxville, TN, USA. [5]Present address: Center for Nanophase Materials Sciences, Oak Ridge National Laboratory, Oak Ridge, TN, USA. [6]These authors contributed equally: Felix Lüpke, Dacen Waters. ✉e-mail: bmhunt@andrew.cmu.edu

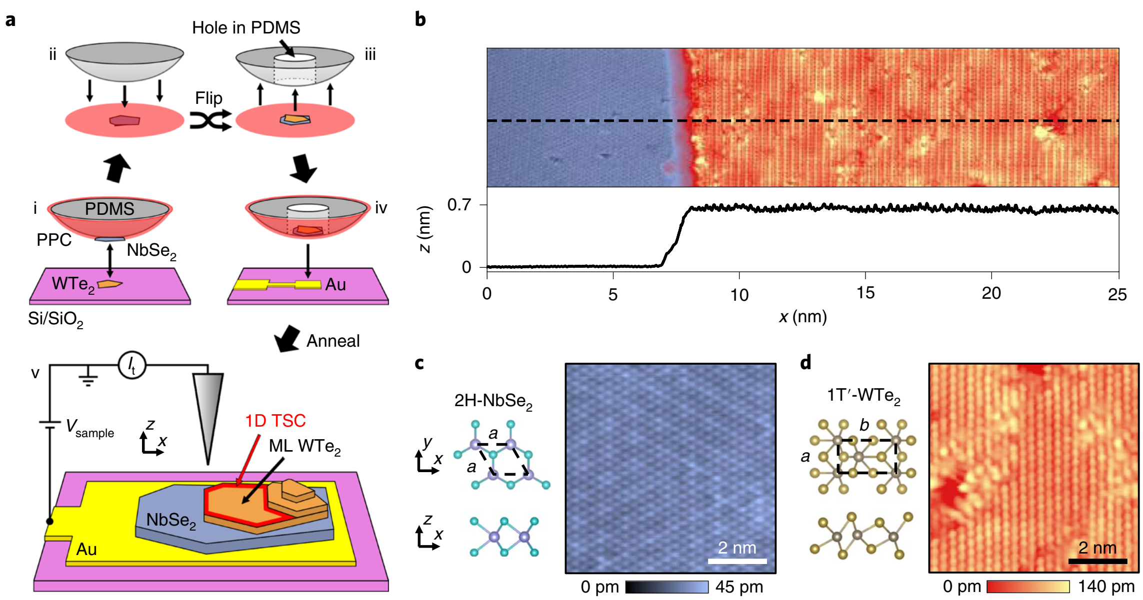

Fig. 1 | Fabrication and morphology of the $WTe_2/NbSe_2$ heterostructure. a, Schematic of the sample fabrication using a dry-transfer flip technique. After assembly of the $NbSe_2/WTe_2$ heterostructure using a polypropylene carbonate/polydimethylsiloxane (PPC/PDMS) stamp (inside a nitrogen-filled glovebox), the PPC film is peeled off, flipped upside down and put onto a new PDMS stamp that has a hole in it. This stamp is used to deterministically place the heterostructure onto prepatterned gold leads without bringing the heterostructure surface into contact with any polymers or solvents. The PPC is then evaporated by annealing under vacuum conditions and the sample is transferred to the STM, all without intermediate air exposure. The proposed continuous 1D topological superconducting state (TSC) is indicated in red in step (v). **b**, STM topography and height profile across the edge of the monolayer (ML) WTe_2 flake ($V_{sample} = 300$ mV, $I_t = 10$ pA). **c**, Atomic structures and atomically resolved STM image of the $NbSe_2$ flake showing the 3×3 charge density wave ($V_{sample} = 300$ mV, $I_t = 35$ pA). **d**, Atomic structures and atomically resolved STM image of monolayer WTe_2 ($V_{sample} = 1$ V, $I_t = 55$ pA), showing different kinds of defect. In **b**, a moiré pattern in the form of diagonal stripes can be seen on the monolayer WTe_2, resulting from the superposition of the two different atomic lattices. Although $NbSe_2$ has a hexagonal unit cell with lattice parameters $a = b = 3.44$ Å, WTe_2 has a rectangular unit cell with lattice parameters $a = 3.48$ Å and $b = 6.28$ Å (**c**,**d**). The moiré pattern, analysed in more detail in Supplementary Section 2, corresponds to a twist angle of ~3°. The topography shown in **b** is representative of the heterostructure cleanliness.

WTe_2 step edge. This feature was recently reported in scanning tunnelling studies of monolayer films of WTe_2 grown on epitaxial graphene substrates. The characteristic signature of the quantum spin Hall edge state is observed on the interior of the monolayer WTe_2, and has a spatial extent of ~1.2 nm, in excellent agreement with previous studies on epitaxial films[1,16]. Based on combined evidence from angle-resolved photoemission spectroscopy and scanning tunnelling measurements in ref. [1], it was concluded that monolayer WTe_2 has a bandgap of 56 ± 14 meV, and that the increased LDOS at the monolayer WTe_2 edge signifies the metallic quantum spin Hall edge state. In our monolayer samples, produced via isolation from bulk crystals rather than molecular beam epitaxy, and on superconducting substrates rather than graphene, we observe the same spectroscopic features, which we attribute to the same quantum spin Hall edge state. Figure 2b shows the dI/dV spectrum on the WTe_2 monolayer (red) and the monolayer edge (orange) at the corresponding positions indicated in Fig. 2a. A non-zero dI/dV signal in the bandgap away from the step edge was proposed to be due to substrate effects (discussed in further detail in the following) and defect states[1]. In addition, tip-induced band bending may play a role in introducing spectral weight in the WTe_2 bandgap (Supplementary Section 3). By comparing the positions of the observed spectral features to epitaxially grown WTe_2 on graphene[1,16] and exfoliated WTe_2 (ref. [22]), we conclude that there is no significant charge transfer from the $NbSe_2$ to the WTe_2. This observation is further supported by our density functional theory calculations of the monolayer $WTe_2/NbSe_2$ heterostructure, which show only minimal modifications of the WTe_2 electronic structure compared to a freestanding WTe_2 monolayer (Supplementary Section 6).

Measurements of the monolayer WTe_2 dI/dV spectrum over a smaller voltage range and with smaller modulation amplitude (Fig. 2c) reveal a new feature that resembles a superconducting gap characterized by a dip in the dI/dV signal at the Fermi energy, with peaks on either side of the gap. When decreasing the measurement temperature from 4.7 K to 2.8 K, the gap deepens and the peaks sharpen, whereas when increasing the temperature the gap vanishes at ~6 K. The evolution of the gap under application of a surface-normal magnetic field at 4.7 K (Fig. 2d) shows that with increasing magnetic field, the gap becomes less deep until it has nearly vanished at 1 T. We find that a fit of the Bardeen–Cooper–Schrieffer (BCS) model describes both the monolayer WTe_2 and the $NbSe_2$ data well (Fig. 3a). For $NbSe_2$, the fit results in a superconducting gap of $\Delta_{NbSe_2} = 0.84 \pm 0.01$ meV, while for the WTe_2 we find $\Delta_{WTe_2}^{(monolayer)} = 0.72 \pm 0.02$ meV. In addition to following the trend of a superconducting gap with applied magnetic field, the vanishing of the gap near 1 T is similar to the Ginzburg–Landau estimate for the upper critical field of bulk $NbSe_2$ (ref. [23]). We conclude that the gap feature observed on the monolayer WTe_2 is indeed a superconducting gap.

To confirm the proximity-induced nature of the observed superconducting gap on the WTe_2, we explore its evolution as a function of WTe_2 thickness. The exfoliation procedure naturally produces terraces of different thickness in our samples, enabling thickness-dependent gap measurements within a single sample. Figure 3b shows the superconducting gap measured on terraces with different numbers of WTe_2 layers N, revealing that the gap decreases with increasing N, as expected for decaying superconducting correlations near the boundary of a superconducting–metal interface[24]. To quantify this behaviour, we fitted the BCS model to each of the spectra in Fig. 3b and plot the extracted gap sizes as filled circles in Fig. 3c. In the thick limit ($N \geq 3$), we find that the observed behaviour shows

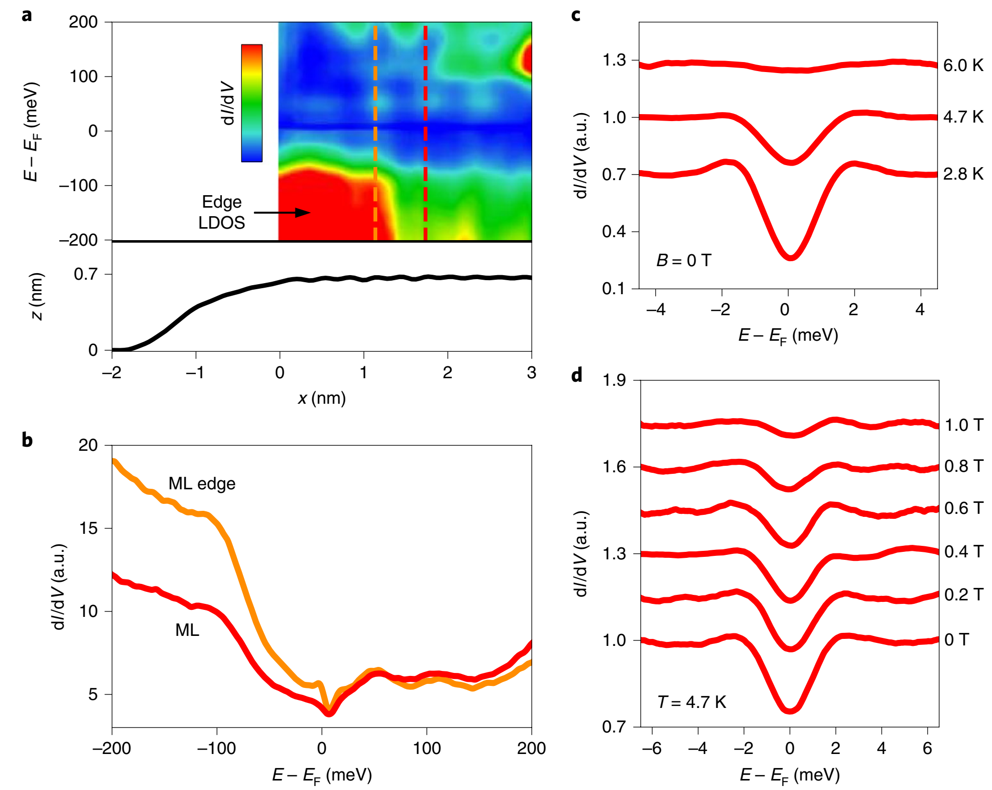

Fig. 2 | Simultaneous presence of the quantum spin Hall edge state and superconducting gap on monolayer WTe_2. a, d*I*/d*V* spectra taken along a line across the step edge of the WTe_2 flake (top) and the horizontally aligned height profile (bottom). **b**, Representative d*I*/d*V* spectra of monolayer WTe_2 away from the monolayer edge (red dashed line in **a**) and increased LDOS at the monolayer edge due to the presence of the quantum spin Hall edge state (orange dashed line in **a**). Modulation amplitude $V_{mod} = 5$ mV. Following the interpretation of ref. [1], the increases in the d*I*/d*V* signal at $E - E_F \approx -50$ meV and $E - E_F \approx 15$ meV correspond to the onset of the WTe_2 valence and conduction bands, respectively, locating E_F in the monolayer WTe_2 bandgap. **c**, Small voltage range d*I*/d*V* spectrum of monolayer WTe_2 at 6 K, 4.7 K and 2.8 K, showing a superconducting gap-like feature ($V_{mod} = 0.1$ mV). Curves are offset for clarity. **d**, Magnetic field dependence of the small voltage range spectrum measured on the WTe_2 monolayer at 4.7 K. Curves are offset for clarity.

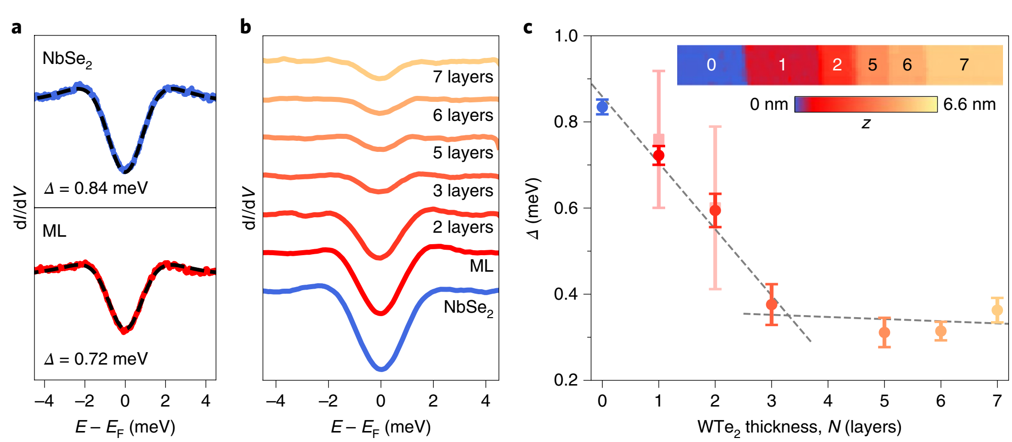

Fig. 3 | Evolution of the superconducting gap with WTe_2 thickness at 4.7 K. a, Fits of the BCS model to the superconducting gap spectra measured on $NbSe_2$ and monolayer WTe_2. **b**, Measurement of the superconducting gap spectrum for WTe_2 layer thicknesses up to seven layers. **c**, Filled circles show the WTe_2 thickness dependence of the superconducting gap size obtained from fitting the spectra in **b** with the BCS gap equation. Filled squares show fits of the monolayer and bilayer spectrum with a more detailed model that includes partial tunnelling into the $NbSe_2$ substrate. Error bars represent ±1 s.d. obtained from the fits. The dashed lines are guides to the eye and indicate two different regimes in which Δ decreases more rapidly for $N < 3$ and more gradually for $N \geq 3$. Inset: large-scale STM image of the WTe_2 flake, showing terraces of different WTe_2 thickness. Scan size, 200 nm × 14 nm. The corresponding number of WTe_2 layers N is indicated for each terrace, where $N = 0$ is the bare $NbSe_2$.

excellent agreement with transport measurements of proximity-induced superconductivity in bulk WTe_2 flakes[24,25], extending the previous studies to the ultra-thin limit (Supplementary Section 5).

For $N < 3$ we observe a more rapid decrease of the extracted gap as a function of N that may be explained by the strong variation of the electronic structure of the WTe_2 in this thickness range, resulting

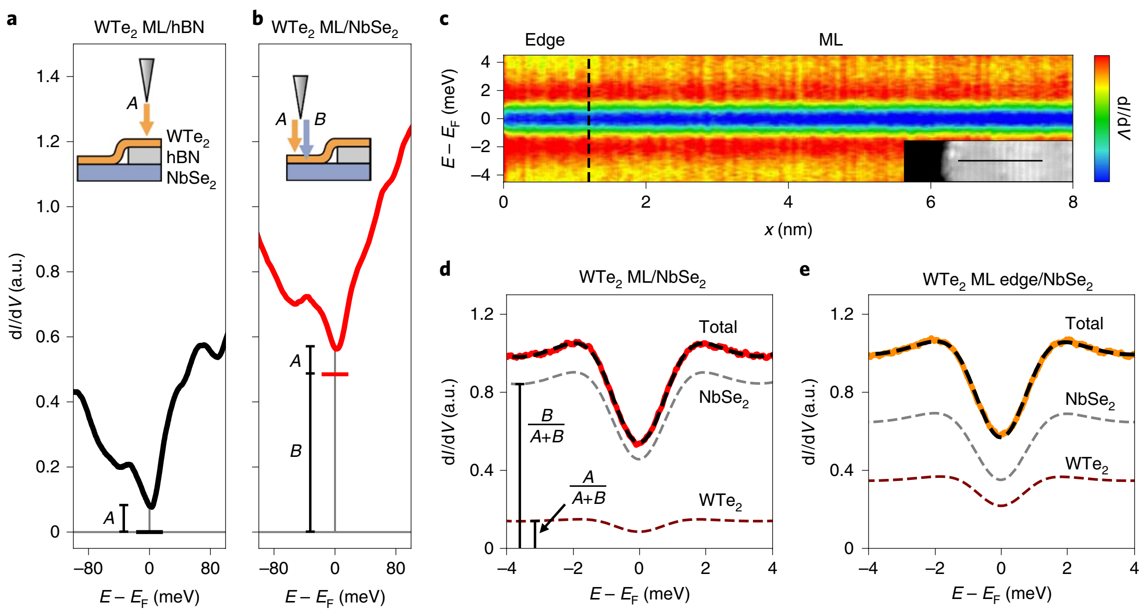

Fig. 4 | Proximity-induced superconducting gap in the quantum spin Hall edge state of monolayer WTe_2 at 2.8 K. a,b, Tunnelling spectrum of WTe_2 on hBN (**a**) and the spectrum of the same WTe_2 flake on $NbSe_2$ (**b**) (for an optical micrograph of the heterostructure see Supplementary Fig. 3). The tunnelling contributions of the WTe_2 and $NbSe_2$ are denoted as *A* and *B*, respectively. **c**, Superconducting gap spectra measured along a line perpendicular to the edge of the WTe_2. Inset: topography and line along which the spectra were taken. Scan size, 16 nm × 4 nm. **d**, Fitting of a representative monolayer WTe_2/$NbSe_2$ tunnelling spectrum. The fractional contribution of tunnelling into WTe_2 is $f_{WTe_2} \equiv A/(A+B) = 0.14 \pm 0.04$. The $NbSe_2$-derived states' contribution is therefore $f_{NbSe_2} = B/(A+B) = 0.86 \pm 0.04$. The model used to fit the data is $(dI/dV)_{Total} = f_{WTe_2}(dI/dV)_{WTe_2} + f_{NbSe_2}(dI/dV)_{NbSe_2}$, using a BCS form for each dI/dV (for details see Supplementary Section 5). The grey and maroon dashed lines indicate the $(dI/dV)_{NbSe_2}$ and $(dI/dV)_{WTe_2}$, the signal due to the proximity-induced superconducting gap in the WTe_2. The size of the induced gap is $\Delta_{WTe_2}^{(monolayer)} = 0.83 \pm 0.08$ meV. **e**, Fitting of the monolayer edge WTe_2/$NbSe_2$ tunnelling spectrum. We use the same gaps(s) found for $NbSe_2$ from **a**, a larger value for f_{WTe_2} determined from the larger tunnelling conductance into the edge state (Fig. 2b), and use $\Delta_{WTe_2}^{(edge)}$ as the fitting parameter. The resulting induced superconducting gap in the WTe_2 quantum spin Hall edge state is $\Delta_{WTe_2}^{(edge)} = 0.75 \pm 0.08$ meV.

in a larger mismatch of the WTe_2 and $NbSe_2$ Fermi surfaces and therefore a stronger dependence of the induced gap on *N* (ref. [26]). For monolayer and bilayer WTe_2, we also consider the possibility of tunnelling spectra being a superposition of tunnelling into WTe_2 and into $NbSe_2$ (Fig. 4b, inset). To isolate the respective contributions, we performed a control experiment on a second sample, in which we placed a 20 nm-thick layer of insulating hexagonal boron nitride (hBN) between the WTe_2 and $NbSe_2$ to locally decouple the WTe_2 (Fig. 4a,b). This allows us to perform a more detailed analysis of the superconducting monolayer WTe_2/$NbSe_2$ spectrum (Fig. 4d) in which we fit a superposition of BCS spectra from the WTe_2 and $NbSe_2$ (for further details, as well as additional measurements of a WTe_2/MoS_2 heterostructure, see Supplementary Section 3). The proximity-induced gaps from fitting the more detailed model are $\Delta_{WTe_2}^{(monolayer)} = 0.76 \pm 0.16$ meV at 4.7 K and 0.83 ± 0.08 meV at 2.8 K. For bilayer WTe_2 on $NbSe_2$, using a similar procedure, we find an induced gap of $\Delta_{WTe_2}^{(bilayer)} = 0.60 \pm 0.19$ meV. In Fig. 3c we also plot the 4.7 K WTe_2 proximity gaps found from this more detailed fitting and find no significant deviation from those previously determined by fitting the single-gap BCS theory. This observation is in qualitative agreement with theory, which predicts the proximity-induced gap to approach that of $NbSe_2$ as the WTe_2 layer thickness goes to zero[24].

Finally, we consider the lateral variation of the superconducting gap from within the monolayer WTe_2 to the region occupied by the edge state. Figure 4c shows dI/dV spectra taken at 2.8 K along a line approaching the physical edge of the WTe_2 monolayer, similar to that shown in Fig. 2a but over a smaller voltage range. We find that the superconducting gap is present throughout the WTe_2 monolayer with only slight changes in the gap width and depth. It is apparent that a superconducting gap is present in the region in which the quantum spin Hall edge state is observed in Fig. 2a (dashed line, Fig. 4c). To determine the fractional contribution of the WTe_2 edge spectrum, in Fig. 4e we perform a similar fit as we did for the spectrum away from the edge (Fig. 4d), using the same absolute $NbSe_2$ background as in Fig. 4d, but using the larger tunnelling conductance of the edge state at the Fermi energy (Fig. 2b). The resulting relative contribution of the edge state is $f_{WTe_2} = 0.33 \pm 0.06$ and the extracted gap size is $\Delta_{WTe_2}^{(edge)} = 0.75 \pm 0.08$ meV.

The observation of a superconducting gap in the edge state of monolayer 1T′-WTe_2 provides strong evidence that we have created a 1D topological superconductor in a van der Waals heterostructure. The topological nature of a superconducting quantum spin Hall edge state could be explicitly demonstrated in an STM measurement by creating a boundary with a portion of the same quantum spin Hall edge state in which a topologically trivial gap has been opened[4]. This would localize Majorana zero modes at the boundary, which can be identified as a zero-bias conductance peak within the superconducting gap[27]. Creating such a boundary is straightforward in the van der Waals material platform, for example by integrating a van der Waals magnetic insulator into the heterostructure shown in Fig. 1a to open a local Zeeman gap. Our work establishes the groundwork for such an experiment with a clear path toward the realization of Majorana quasiparticles. In addition, the method of sample preparation outlined in this work may be easily adapted to numerous experiments involving surface-probe studies or air-sensitive materials.

Online content

Any methods, additional references, Nature Research reporting summaries, source data, extended data, supplementary information, acknowledgements, peer review information; details of author contributions and competing interests; and statements of data and code availability are available at https://doi.org/10.1038/s41567-020-0816-x.

Received: 9 August 2019; Accepted: 29 January 2020;
Published online: 16 March 2020

References

1. Tang, S. et al. Quantum spin Hall state in monolayer $1T_2$-WTe_2. *Nat. Phys.* **13**, 683–687 (2017).
2. Fei, Z. et al. Edge conduction in monolayer WTe_2. *Nat. Phys.* **13**, 677–682 (2017).
3. Wu, S. et al. Observation of the quantum spin Hall effect up to 100 kelvin in a monolayer crystal. *Science* **359**, 76–79 (2018).
4. Alicea, J. New directions in the pursuit of majorana fermions in solid state systems. *Rep. Prog. Phys.* **75**, 076501 (2012).
5. Kitaev, A. Y. Unpaired majorana fermions in quantum wires. *Phys. Uspekhi* **44**, 131–136 (2001).
6. Fu, L. & Kane, C. L. Superconducting proximity effect and majorana fermions at the surface of a topological insulator. *Phys. Rev. Lett.* **100**, 096407 (2008).
7. DasSarma, S., Freedman, M. & Nayak, C. Majorana zero modes and topological quantum computation. *npj Quantum Inf.* **1**, 15001 (2015).
8. Sato, M. & Ando, Y. Majorana zero modes and topological quantum computation. *Rep. Prog. Phys.* **80**, 076501 (2017).
9. Maeno, Y., Kittaka, S., Nomura, T., Yonezawa, S. & Ishida, K. Evaluation of spin-triplet superconductivity in $Sr_2 RuO_4$. *J. Phys. Soc. Jpn* **81**, 011009 (2012).
10. Fu, L. & Kane, C. L. Josephson current and noise at a superconductor/quantum-spin-Hall-insulator/superconductor junction. *Phys. Rev. B* **79**, 161408 (2009).
11. Wang, M.-X. et al. The coexistence of superconductivity and topological order in the Bi_2Se_3 thin films. *Science* **336**, 52–55 (2012).
12. Sun, H.-H. et al. Majorana zero mode detected with spin selective Andreev reflection in the vortex of a topological superconductor. *Phys. Rev. Lett.* **116**, 257003 (2016).
13. Hart, S. et al. Induced superconductivity in the quantum spin Hall edge. *Nat. Phys.* **10**, 638–643 (2014).
14. Bocquillon, E. et al. Gapless Andreev bound states in the quantum spin Hall insulator HgTe. *Nat. Nanotechnol.* **12**, 137–143 (2016).
15. Jia, Z.-Y. et al. Direct visualization of a two-dimensional topological insulator in the single-layer $1T_2$-WTe_2. *Phys. Rev. B* **96**, 041108 (2017).
16. Peng, L. et al. Observation of topological states residing at step edges of WTe_2. *Nat. Commun.* **8**, 659 (2017).
17. Shi, Y. et al. Imaging quantum spin Hall edges in monolayer WTe_2. *Sci. Adv.* **5**, eaat8799 (2019).
18. Qian, X., Liu, J., Fu, L. & Li, J. Quantum spin Hall effect in two-dimensional transition metal dichalcogenides. *Science* **346**, 1344–1347 (2014).
19. Fatemi, V. et al. Electrically tunable low-density superconductivity in a monolayer topological insulator. *Science* **362**, 926–929 (2018).
20. Sajadi, E. et al. Gate-induced superconductivity in a monolayer topological insulator. *Science* **362**, 922–925 (2018).
21. Zeng, Y. et al. High-quality magnetotransport in graphene using the edge-free Corbino geometry. *Phys. Rev. Lett.* **122**, 137701 (2019).
22. Cucchi, I. et al. Microfocus laser angle-resolved photoemission on encapsulated mono-, bi- and few-layer $1T_2$-WTe_2. *Nano Lett.* **19**, 554–560 (2019).
23. Garoche, P., Veyssié, J. J., Manuel, P. & Molinié, P. Experimental investigation of superconductivity in 2H-$NbSe_2$ single crystal. *Solid State Commun.* **19**, 455–460 (1976).
24. Huang, C. et al. Inducing strong superconductivity in WTe_2 by a proximity effect. *ACS Nano* **12**, 7185–7196 (2018).
25. Li, Q. et al. Proximity-induced superconductivity with subgap anomaly in type II Weyl semi-metal WTe_2. *Nano Lett.* **18**, 7962–7968 (2018).
26. Reeg, C. R. & Maslov, D. L. Hard gap in a normal layer coupled to a superconductor. *Phys. Rev. B* **94**, 020501 (2016).
27. Jäck, B. et al. Observation of a Majorana zero mode in a topologically protected edge channel. *Science* **364**, 1255–1259 (2019).

Methods

WTe_2 and $NbSe_2$ were exfoliated onto SiO_2 in a nitrogen-filled glovebox. A WTe_2 flake with regions of different thickness was transferred onto a (20 ± 1) nm-thick $NbSe_2$ flake using the technique depicted in Fig. 1a. At this thickness, the electronic properties of the $NbSe_2$ are bulk-like and the critical temperature below which the $NbSe_2$ becomes superconducting is $T_c \approx 7$ K (ref. [28]). For optical images of the sample and further details about the sample fabrication, see Supplementary Section 1. The STM tip was approached to the WTe_2/$NbSe_2$ heterostructure using a capacitive technique adapted from ref. [29]. The commercial CreaTec STM helium bath temperature was 4.2 K with the ability to intermittently reach ~1 K by pumping on the cryostat. The resulting STM temperatures were 4.7 K and 2.8 K, respectively, due to vibration isolation and optical access. The STM was equipped with an electrochemically etched tungsten tip, which was indented into gold before and between measurements. The lock-in frequency was set to $f = 925$ Hz in all dI/dV measurements. All superconducting gap measurements were performed at $V_{sample} = 5$ mV with $V_{mod} = 100\,\mu$V peak-to-peak and $I_t = 100$ pA, except in Fig 2e, where $V_{sample} = 10$ mV. The spectra in Fig. 2a,b were acquired using $V_{mod} = 5$ mV. In Fig. 4a $V_{sample} = 300$ mV, $I_t = 100$ pA and $V_{mod} = 5$ mV and in Fig 4b $V_{sample} = 300$ mV, $I_t = 110$ pA and $V_{mod} = 10$ mV. For quantitative comparison, the spectra in Fig. 4a,b were normalized to I_t and V_{mod}.

Data availability

The data represented Figs. 1, 2, 3 and 4 are available as Source Data with the online version of the paper. All other data that support the plots within this paper and other findings of this study are available from the corresponding author upon reasonable request.

References

28. Khestanova, E. et al. Unusual suppression of the superconducting energy gap and critical temperature in atomically thin $NbSe_2$. *Nano Lett.* **18**, 2623–2629 (2018).
29. Li, G., Luican, A. & Andrei, E. Y. Self-navigation of a scanning tunneling microscope tip toward a micron-sized graphene sample. *Rev. Sci. Instrum.* **82**, 073701 (2011).

Acknowledgements

We thank D. Xiao, D. Cobden and X. Xu for helpful discussions and N. Speeney and N. Iskos for assistance in the laboratory. B.M.H. was supported by the Department of Energy under the Early Career award programme (DE-SC0018115). Crystal growth and characterization at ORNL were supported by the US Department of Energy, Office of Science, Basic Energy Sciences, Division of Materials Sciences and Engineering. We thank the Pennsylvania State University Two-Dimensional Crystal Consortium—Materials Innovation Platform (2DCC-MIP), which is supported by NSF DMR-1539916, for supplying further 2D materials. F.L. and D.W. were supported by the NSF DMR-1809145 for STM measurements. We acknowledge NSF DMR-1626099 for acquisition of the STM instrument. S.C.d.l.B. was supported by the Department of Energy (DE-SC0018115) for fabrication of proximity-effect van der Waals heterostructures. Density functional theory calculations were supported by the Department of Energy under grant no. DE-SC0014506.

Author contributions

F.L., D.W., R.M.F. and B.M.H. designed the experiment. F.L. and D.W. acquired the experimental data and F.L., D.W. and R.M.F. analysed it. F.L., D.W. and S.C.d.l.B. fabricated the samples. F.L., D.W., S.C.d.l.B., R.M.F. and B.M.H. wrote the manuscript, and all authors commented on it. J.Y. grew the WTe_2 crystals. D.G.M. provided other van der Waals crystals used in this study. M.W. performed density functional theory calculations. R.M.F. and B.M.H. supervised the project.

Competing interests

The authors declare no competing interests.

Additional information

Supplementary information is available for this paper at https://doi.org/10.1038/s41567-020-0816-x.

Correspondence and requests for materials should be addressed to B.M.H.

Peer review information *Nature Physics* thanks Feng Miao and the other, anonymous, reviewer(s) for their contribution to the peer review of this work.